Influence of Cooling Rate After Destabilization on Microstructure and Hardness of a High-Cr Cast Iron

CHARLINE LE NUÉ, SANTIAGO CORUJEIRA GALLO, ALIREZA VAHID, MEHDI TAHERISHARGH, HOOYAR ATTAR, DANIEL FABIJANIC, and MATTHEW BARNETT

This study investigates the impact of cooling rate after destabilization at 980 °C on the microstructure of 23 wt pct Cr–2.7wt pct C hypoeutectic high-Cr cast iron. Lowering cooling rate intensifies the secondary carbides formation, depleting carbon in austenite. This raises the martensite start temperature and lowers the bulk hardness. We thereby provide evidence explaining the origin of the sensitivity to cooling rate in high-Cr cast irons.

https://doi.org/10.1007/s11661-024-07393-w

HIGH-CHROMIUM cast irons (HCCI) are widely used in minerals and mining industries for applications requiring high hardness and wear resistance.[1–4] In the as-cast state, their microstructure typically consists of eutectic carbides (EC) M_7C_3 in a matrix of austenite, which may remain stable or partially transformed (depending on the composition and the solidification rate).[1,5–9] HCCI are generally used in the heat-treated state, improving wear properties. The most commonly used heat treatment, termed 'destabilization' treatment because of its influence on the propensity of austenite to form martensite upon cooling, is usually conducted between 800 °C and 1100 °C. The heat treatment leads to the precipitation of secondary carbides (SC), resulting in the depletion of alloying elements from the austenitic matrix. This compositional modification favors the transformation of austenite into martensite during the subsequent cooling.[10–12] The component is held at high temperature for between 1 and 6 hours and then quenched to room temperature,[10,13–17] often by air cooling. A fast cooling rate (> 200 °C/minute) is not recommended due to casting crack risk. Understanding the impact of cooling rate after destabilization treatment on the microstructure and properties is essential as, in practice, it cannot generally be perfectly controlled, especially in large components. Consequently, the sensitivity to cooling rate has the potential to result in microstructure and property gradients over a component geometry.

The influence of destabilization treatment on the microstructure and hardness of HCCI has been widely studied.[10–14,17–22] However, very few studies have investigated the influence of cooling rate. Li *et al.*[23] studied the effect of quenching medium (water, water + 10 pct PAG coolant, and water + 20 pct PAG coolant) on the hardness of 2.14C–14.7Cr (wt pct) HCCI after destabilization at 950 °C for 2 hours. Their results show that the water-cooled specimen (fastest cooling rate) had the highest hardness (66.2 HRC), whereas the specimen treated with 20 pct PAG (slowest cooling rate) had the lowest hardness (58.1 HRC). However, this study does not provide detailed correlative microstructure analyses to explain the variation in hardness. Tupaj *et al.*[24] studied the effect of cooling rate after destabilization (at 1000 °C for 30 minutes) of a 3.5C–15Cr–1.1Si–0.65Mn 0.5Mo–0.3Ni (wt pct) HCCI and found that martensite start temperature (M_s) strongly depends on the quenching medium (air, liquid nitrogen, or water). The authors assert that the cooling rate below 400 °C determines the M_s temperature; however, the basis for this was unclear. It is worth emphasizing that cooling rates were not controlled and continuously varied; the authors provide average cooling rate values over two temperature ranges, 800 °C to 400 °C and 400 °C-M_s (liquid nitrogen: 14.8 °C/minute, 6 °C/minute; water: 20.9 °C/minute, 3.8 °C/minute; air 6.9 °C/minute, 1.9 °C/minute, respectively). This lack of cooling rate control complicates drawing definitive conclusions about the effects on the microstructure and hardness. Nevertheless, the

CHARLINE LE NUÉ, SANTIAGO CORUJEIRA GALLO, ALIREZA VAHID, DANIEL FABIJANIC, and MATTHEW BARNETT are with the Institute for Frontier Materials, Deakin University, Waurn Ponds, VIC 3216, Australia. Contact e-mail: c.lenue@deakin.edu.au MEHDI TAHERISHARGH AND HOOYAR ATTAR are with the Bradken, 20 McIntosh Drive, Mayfield West, NSW 2304, Australia.
Manuscript submitted January 31, 2024; accepted March 21, 2024.
Article published online April 8, 2024

authors observed a broad trend that reducing the cooling rate resulted in higher M_s values, and the slow-cooled air-cooled specimen exhibited the lowest hardness values. Tupaj *et al.* suggest that carbide formation may have occurred during cooling to a greater extent in the air-cooled samples. However, no microstructure observation or quantification is provided to test this hypothesis.

Gonzales-Pociño *et al.*,[25] in their study on 18Cr–3C–2Mo–1.2Si–0.8Mn (wt pct) HCCI, evaluated the influence of holding time from 4 to 24 hours at 1000 °C, followed by air or oil cooling. They observed that the hardness of oil-quenched samples was greater than those quenched in air. The authors report that a greater density of SC was obtained with increasing holding time at 1000 °C. They also reported that additional SC precipitation occurs at 400 °C to 600 °C for air-cooled samples; however how this was determined is unclear. Other authors have also suggested that further SC formation could occur during cooling after destabilization treatment.[16,19] Unfortunately, these prior studies on cooling rate effects did not include sufficient microstructure characterization or variation of controlled cooling rate for process-microstructure relations to be understood. The present study aims to clarify the impact of the cooling rate applied after destabilization treatment on the microstructure and hardness of a hypoeutectic HCCI.

The alloy grade investigated, a hypoeutectic high-chromium cast iron containing 23 wt pct Cr–2.7 wt pct C (+ Mo), is classified as Class III, type A, HCCI according to ASTM A532 ''Standard Specification for Abrasion-Resistant Cast Irons''. The material was cast as a 300 kg ingot (trapezoidal prism – 500 mm high, 350 mm wide, and bases of length 358 and 100 mm) was prepared by sand mould casting and cooling naturally to ambient temperature. All specimens were extracted from the same location (edge region of the top section) using wire-electrode cutting. Heat treatments were performed using a quench dilatometer (TA Instruments DIL 805 A/D dilatometer). Rod samples of 10 mm height and 4 mm diameter were heated up to 980 °C at a rate of 5 °C/minute (to approximate industrial heating rates), held for 5 h and cooled to room temperature (RT) at various cooling rates – 2.5 °C/minute, 5 °C/minute, 10 °C/minute, 20 °C/minute, 80 °C/minute and 600 °C/minute. The microstructure was examined with a Jeol JSM 7800F field emission gun scanning electron microscope (FEG-SEM) after a metallographic preparation to a final polish with colloidal silica suspension (0.06 μm). The specimens were examined using back-scattering electron (BSE) imaging. The fraction of EC and SC was determined from image analysis using ImageJ software from an average of 10 micrographs. The carbon concentration of the austenite was estimated from the lattice parameter determined using X-ray diffraction (XRD). The analyses were conducted on a PANalytical X'Pert MRD XL laboratory diffractometer using a Cu Kα radiation, an acceleration voltage of 40 kV, a 40 mA tube current, a 2θ range from 35 to 95 deg, and a step size of 0.02 deg. Vickers hardness of heat-treated samples was measured using a load of 10 kgf, and the mean values were obtained from 15 measurements.

The as-cast microstructure consisted of primary austenite dendrites, M_7C_3 EC (M = Cr, Fe), and martensite surrounding the EC. The EC and austenite volume fractions were 28.9 ± 0.9 and 10.6 ± 0.6 pct, respectively. After destabilization treatment and for all cooling rates investigated, the dendritic regions comprise a martensitic matrix and a mixture of M_7C_3 and $M_{23}C_6$ SC (Figures 1(a) and (b)). The interdendritic regions were composed of M_7C_3 EC and martensite. We can differentiate SC in the back-scattered electron composition-contrast (BSE) images: $M_{23}C_6$ corresponds to the light grey particles, whereas M_7C_3 appear darker. More details about the identification and characterization of SC are reported in Reference 26. Due to the sub-micron size of $M_{23}C_6$ SC and the low contrast difference with the matrix, we could only quantify the M_7C_3 SC. The results, given in Figure 1(c), show that the volume percentage of M_7C_3 SC notably changes with the cooling rate.

Dilatometry revealed that martensite transformation is the only notable phase change upon cooling (Figure 2(a)). In Figure 2(b), the dilatometry curves are shifted along the y-axis to facilitate their comparison, and tangents are added. This reveals a slight deviation from linearity between ~ 700 °C and 980 °C, which may indicate carbide precipitation during cooling. This deviation from linearity became less distinctive with an increase in the cooling rate; it appears to be absent for the fastest cooling rate of 600 °C/minute. The martensite start (M_s) temperature is determined using the tangent method (according to ASTM A1033 – 18) for all the cooling rates investigated. The dependence of M_s on the cooling rate is given in Figure 2(c). The results show a significant decrease in M_s when the cooling rate increases. The M_s stabilizes at ~ 180 °C for the highest cooling rates.

The X-ray diffraction patterns, shown in Figure 3, confirm the presence of martensite, austenite, M_7C_3 and $M_{23}C_6$ carbides (M = Cr, Fe). The difficulty in identifying austenite due to a low phase fraction and overlapping peaks should be noted, and SC are not distinguishable due to commonality with EC phase (M_7C_3) peaks and low volume fractions ($M_{23}C_6$). Based on the comparison with the pattern corresponding to the as-cast state (AC), we can qualitatively state that the retained austenite content is << 10 vol pct. Split peaks at ~ 2θ = 44 and 82 deg provide evidence for the tetragonality of the martensite after destabilization treatment.[27–29] This is particularly noticeable for the highest cooling rates. Lattice parameters of the martensite are determined using Rietveld refinement. The carbon content in the martensite is estimated from the c/a ratio obtained using the relation proposed by Bhadeshia and Honeycombe[30]:

$$c/a = (1 + 0.045\,\text{wt pct}C) \quad [1]$$

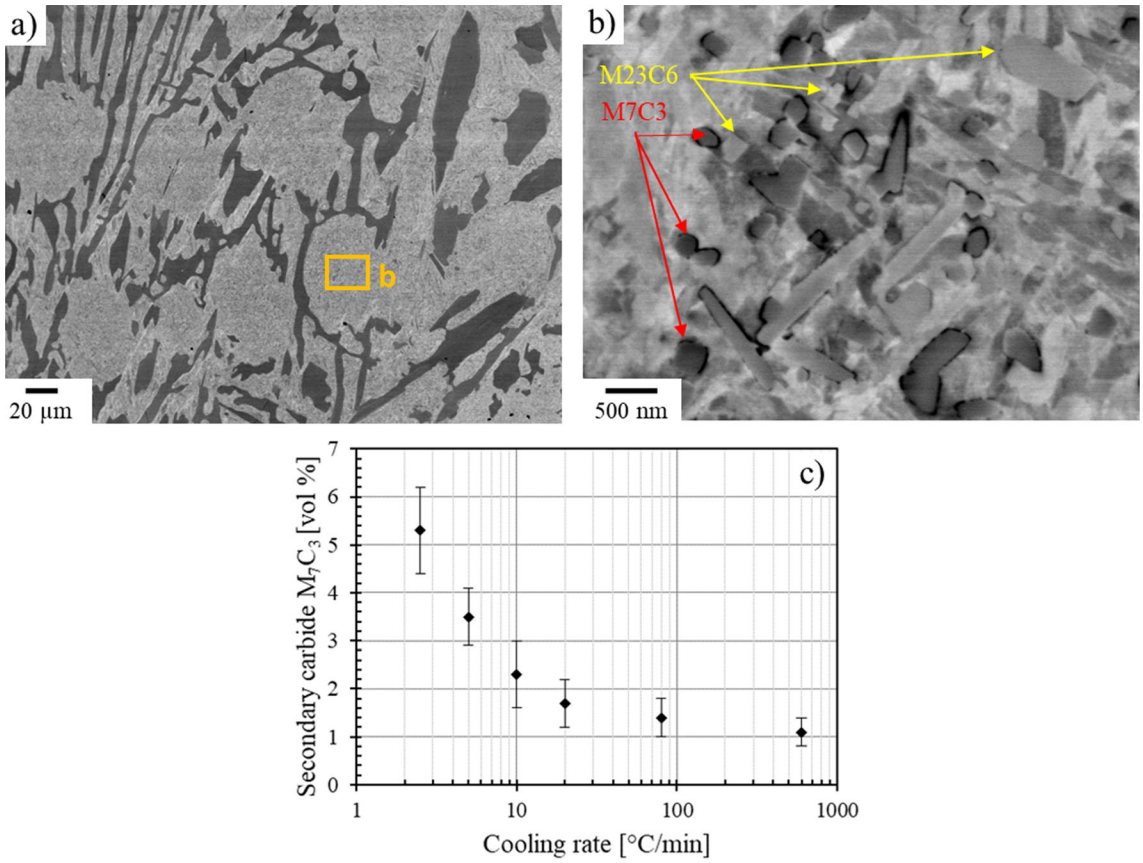

Fig. 1—Back-scattered electron images showing the microstructure after destabilization at 980 °C for 5 h followed by cooling at a rate of 2.5 °C/min (*a*) general microstructure consisting of martensitic dendrites and M_7C_3 EC in the interdendritic region (*b*) higher magnification of dendritic region showing SC. (*c*) Influence of cooling rate after destabilization treatment on proportion of SC.

For the lowest cooling rate, the spitting of the peaks is not so obvious, and it is particularly challenging to access the c/a ratio. Hence, to have another point of comparison, the carbon content is estimated from M_s values, measured experimentally, using the equation developed by Barbier[31]:

$$\begin{aligned} Ms = {} & 545 - 601.2 \times (1 - Exp(-0.868\text{C pct})) \\ & - 34.4\text{Mn pct} - 17.7\text{Si pct} - 9.2\text{pctCr} \\ & - 17.3\text{pctNi} - 15.4\text{Mo pct} + 10.8\text{V pct} \\ & + 4.7\text{Co pct} - 1.4\text{Al pct} - 16.3\text{Cu pct} \\ & - 361\text{Nb pct} - 2.44\text{Ti pct} - 344\text{B pct} \end{aligned} \quad [2]$$

We assume that all elements are soluble in the matrix. Thus, the matrix composition is supposed to be equal to the nominal composition, except for the carbon and chromium contents. The composition of chromium in the matrix is estimated by mass balance from the composition and quantification of carbides obtained experimentally (EC and SC). For EC, the chromium concentration is ~ 63 wt pct, determined from EDS. For M_7C_3 and $M_{23}C_6$ SC, chromium content equals ~ 29 wt pct and ~ 50 wt pct, respectively; the authors previously determined these values in Reference 26. Solute carbon estimations obtained using both approaches are presented in Figure 4. There is an increase in carbon content in the matrix with an increasing cooling rate. The estimated carbon content in the matrix for the two highest cooling rates studied, 80 °C/minute and 600 °C/minute, are relatively similar. We also note a good agreement between the C values estimated from XRD and M_s.

This work extends the knowledge about the effect of cooling rate after destabilization treatment on the microstructure and properties of HCCI. The present study confirms that further precipitation of SC occurs during cooling. Nevertheless, the critical range of temperatures in which precipitation occurs is higher in the present study (700 °C to 980 °C) compared to those proposed, but not experimentally verified, by Tupaj *et al.* (< 400 °C).[24] This precipitation explains the carbon reduction in the matrix obtained experimentally and, consequently, the M_s evolution with the cooling rate. The higher volume fraction of SC obtained for the slow cooling rate leads to the reduction of carbon and other alloying elements in the matrix, explaining the rise of M_s temperature. Similar results are found in the literature for martensitic stainless steels,[32–34] micro-alloyed steels,[35] and chromium hot-work tool steels.[36] Ning *et al.*,[36] in their study of AISI H13 (4Cr5MoSiV1), found that both volume fraction and size of carbides decrease with the increase of the cooling rate after austenitization. Souza *et al.*,[35] in a study of

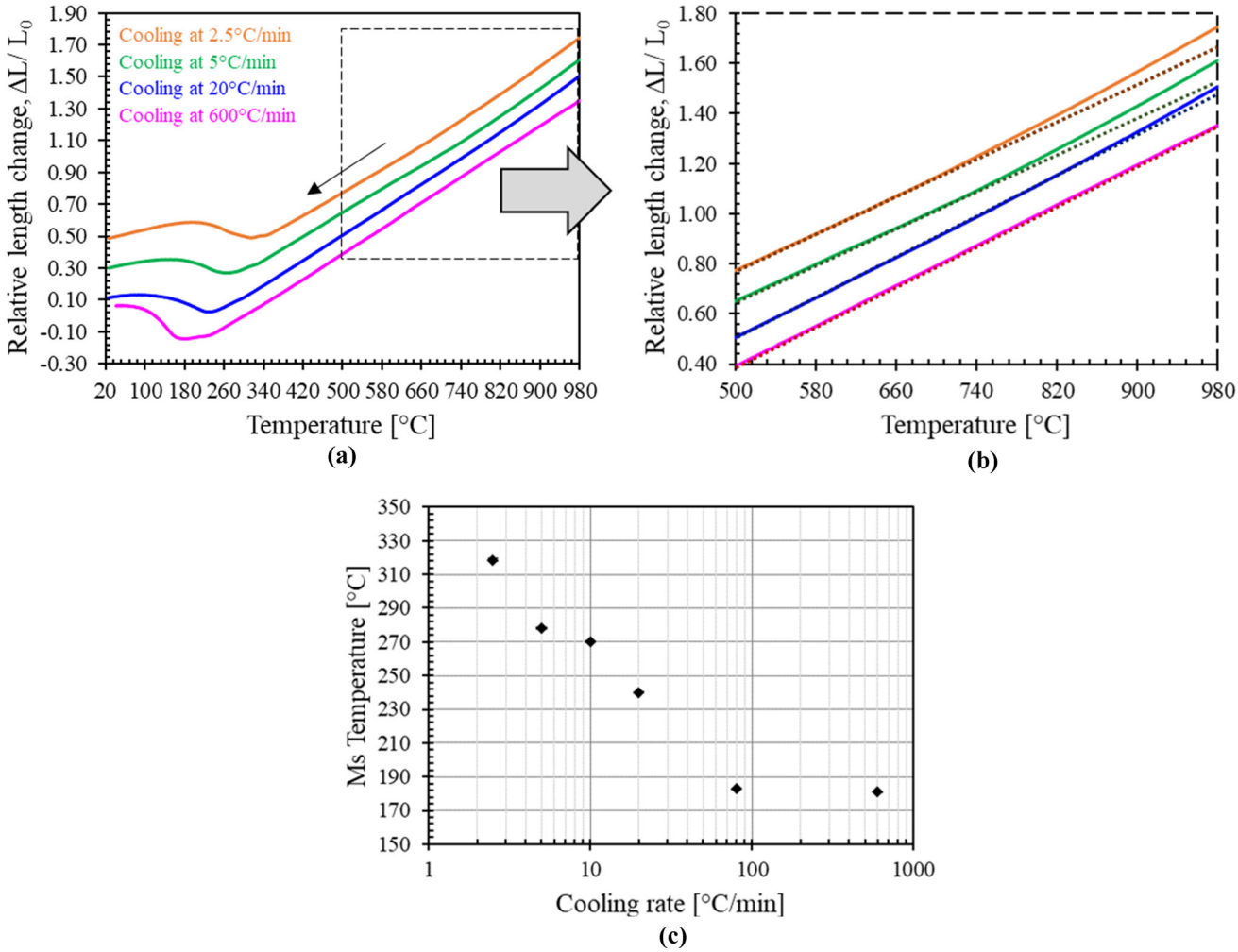

Fig. 2—Dilatometry results showing (*a*) and (*b*) continuous cooling curves after destabilization at 980 °C and (*c*) the relationship between M_s and cooling rate.

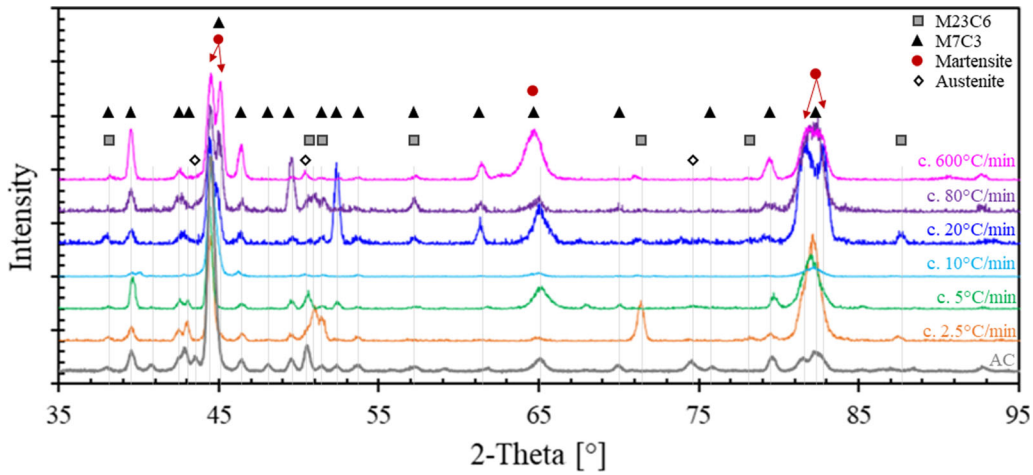

Fig. 3—XRD patterns obtained after destabilization at 980 °C/5 h, followed by cooling at 2.5 to 600 °C/min.

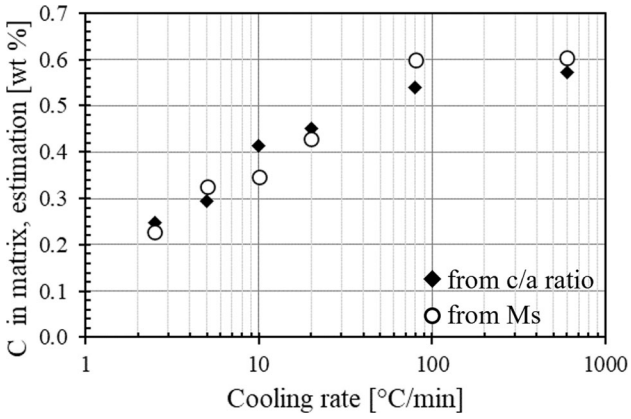

Fig. 4—Carbon estimation in the martensite phase from the c/a ratio (obtained from XRD) and from M_s values obtained from dilatometry, plotted against the cooling rate applied after destabilization treatment.

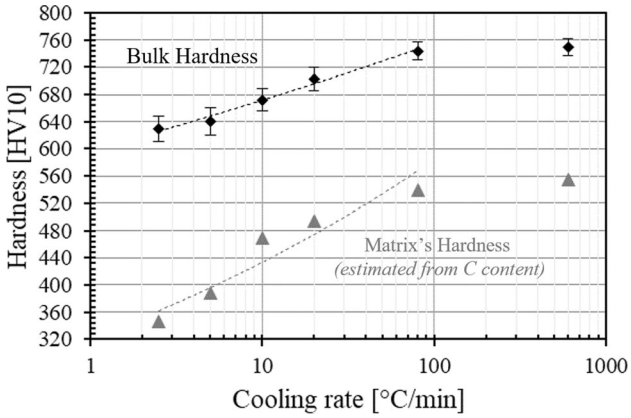

Fig. 5—Hardness evolution with cooling rate after destabilization at 980 °C during 5 h.

Mo–Cr micro-alloyed steel, conclude that a slow cooling rate directly affects austenite stability. The authors suggest that carbide precipitation modifies the austenite chemical composition for a lower cooling rate, resulting in increased M_s temperature.

The relationship between bulk hardness and cooling rate is given in Figure 5. Hardness increases with cooling rate, reaching a plateau at 80 °C/minute. The contribution of the matrix hardness is estimated from carbon content determined experimentally, using the well-known relationship between carbon solubilized in martensite and hardness.[37–39] Values are normalized by the martensite volume fraction and added to Figure 5. The matrix hardness increase is explained largely by the higher carbon content, although it is well-known that SC also contributes to the hardness.[1,6,10,40] Clearly, the increase in SC formation induced by a reduction of cooling rate is not able to compensate for the drop in hardness due to the decrease in carbon content of the matrix.

In summary, the present study provides evidence, through correlative technique, that further precipitation of secondary carbides occurs during cooling after destabilization of hypoeutectic high-Cr cast irons. This validates the hypothesis that by decreasing the cooling rate, the austenitic solid solution becomes impoverished in carbon, raising the M_s temperature and reducing martensite hardness. Furthermore, this impacts significantly on the bulk hardness, thereby explaining the origin of the sensitivity to the cooling rate of these alloys.

ACKNOWLEDGMENTS

This research was conducted by the Australian Research Council Industrial Transformation Training Centre in Alloy Innovation for Mining Efficiency (project number IC160100036) and funded by the Australian Government. The authors also acknowledge the microstructural characterization with the help of Deakin University's Advanced Characterization Facility.

FUNDING

Open Access funding enabled and organized by CAUL and its Member Institutions.

DATA AVAILABILITY

Research data in this work are available by sending direct requests to the corresponding author.

CONFLICT OF INTEREST

On behalf of all authors, the corresponding author states that there is no conflict of interest.

OPEN ACCESS

REFERENCES

1. C.P. Tabrett, I.R. Sare, and M.R. Ghomashchi: *Int. Mater. Rev.*, 1996, vol. 41, pp. 59–82. https://doi.org/10.1179/imr.1996.41.2.59.
2. C.P. Tabrett and I.R. Sare: *Wear*, 1997, vol. 203–204, pp. 206–19. https://doi.org/10.1007/BF02664672.
3. K.-H.Z. Gahr and G.T. Eldis: *Wear*, 1980, vol. 64, pp. 175–94. https://doi.org/10.1016/0043-1648(80)90101-5.
4. A. Bedolla-Jacuinde, R. Correa, I. Mejía, J.G. Quezada, and W.M. Rainforth: *Wear*, 2007, vol. 263, pp. 808–20. https://doi.org/10.1016/j.wear.2006.12.011.
5. Ö.N. Doğan, J.A. Hawk, and G. Laird: *Metall. Mater. Trans. A*, 1997, vol. 28A, pp. 1315–28. https://doi.org/10.1007/s11661-997-0267-3.
6. A. Wiengmoon, J.T.H. Pearce, and T. Chairuangsri: *Mater. Chem. Phys.*, 2011, vol. 125, pp. 739–48. https://doi.org/10.1016/j.matchemphys.2010.09.064.
7. A. Bedolla-Jacuinde: *Int. J. Cast Met. Res.*, 2001, vol. 13, pp. 343–61. https://doi.org/10.1080/13640461.2001.11819416.
8. B.H. Hinckley, K.F. Dolman, R. Wuhrer, A. Ray, and W. Yeung: *Microsc. Microanal.*, 2008, vol. 14, pp. 550–51. https://doi.org/10.1017/S1431927608084067.
9. N.H.K. Luan, K. Koizumi, K. Mizuno, Y. Yamada, and T. Okuyama: *Mater. Trans.*, 2019, vol. 60, pp. 2475–80. https://doi.org/10.2320/matertrans.F-M2019844.
10. A. Bedolla-Jacuinde, L. Arias, and B. Hernández: *J. Mater. Eng. Perform.*, 2003, vol. 12, pp. 371–82. https://doi.org/10.1361/105994903770342881.
11. H. Gasan and F. Erturk: *Metall. Mater. Trans. A*, 2013, vol. 44A, pp. 4993–5005. https://doi.org/10.1007/s11661-013-1851-3.
12. A. Wiengmoon, T. Chairuangsri, A. Brown, R. Brydson, D.V. Edmonds, and J.T.H. Pearce: *Acta Mater.*, 2005, vol. 53, pp. 4143–54. https://doi.org/10.1016/j.actamat.2005.05.019.
13. C.P. Tabrett and I.R. Sare: *Scripta Mater.*, 1998, vol. 38, pp. 1747–53. https://doi.org/10.1016/S1359-6462(98)00118-3.
14. V. Efremenko, K. Shimizu, and Y. Chabak: *Metall. Mater. Trans. A*, 2013, vol. 44A, pp. 5434–46. https://doi.org/10.1007/s11661-013-1890-9.
15. J. Wang, Z. Sun, R. Zuo, C. Li, B. Shen, S. Gao, and S. Huang: *J. Mater. Eng. Perform.*, 2006, vol. 15, pp. 316–19. https://doi.org/10.1361/105994906X108602.
16. J. Wang, C. Li, H. Liu, H. Yang, B. Shen, S. Gao, and S. Huang: *Mater Charact*, 2006, vol. 56, pp. 73–78. https://doi.org/10.1016/j.matchar.2005.10.002.
17. A.E. Karantzalis, A. Lekatou, and E. Diavati: *J. Mater. Eng. Perform.*, 2009, vol. 18, pp. 1078–85. https://doi.org/10.1007/s11665-009-9353-6.
18. G.L.F. Powell and G. Laird: *J. Mater. Sci.*, 1992, vol. 27, pp. 29–35. https://doi.org/10.1007/BF02403640.
19. M.A. Guitar, U.P. Nayak, D. Britz, and F. Mücklich: *Int. J. Met.*, 2020, vol. 14, pp. 755–65. https://doi.org/10.1007/s40962-020-00407-4.
20. H.D.T. Hong, H.N. Hong, M.N. Ngoc, and Q.H.T. Ngoc: *ISIJ Int.*, 2021, vol. 61, pp. 1660–68. https://doi.org/10.2355/ISIJINTERNATIONAL.ISIJINT-2020-581.
21. A. Wiengmoon, N. Tareelap, S. Imurai, T. Chairuangsri, and J.T.H. Pearce: *Solid State Phenom.*, 2018, vol. 283, pp. 95–100. https://doi.org/10.4028/www.scientific.net/SSP.283.95.
22. K. Kishore, U. Kumar, N. Dinesh, and M. Adhikary: *J. Fail. Anal. Prev.*, 2020, vol. 20, pp. 249–60. https://doi.org/10.1007/s11668-020-00836-7.
23. Yi. Li, P.-X. Zhu, C. Tang, and Z. Sun: *Crystals*, 2022, vol. 12, p. 1332. https://doi.org/10.3390/cryst12101332.
24. M. Tupaj, A.W. Orłowicz, A. Trytek, M. Mróz, G. Wnuk, and A.J. Dolata: *Materials (Basel)*, 2020, vol. 13, pp. 1–13. https://doi.org/10.3390/ma13122760.
25. A. Gonzalez-Pocino, F. Alvarez-Antolin, and J. Asciensio-Lozano: *Metals (Basel)*, 2019, vol. 9, p. 522.
26. C. Le Nué, S.C. Gallo, A. Vahid, J. Wang, M. Taherishargh, H. Attar, D. Fabijanic, and M. Barnett: *Metall. Mater. Trans. A*, 2023, https://doi.org/10.1007/s11661-023-07216-4.
27. N. Maruyama, S. Tabata, and H. Kawata: *Metall. Mater. Trans. A*, 2020, vol. 51A, pp. 1085–97. https://doi.org/10.1007/s11661-019-05617-y.
28. L. Xiao, Z. Fan, Z. Jinxiu, Z. Mingxing, K. Mokuang, and G. Zhenqi: *Phys. Rev. B*, 1995, vol. 52, pp. 9970–78. https://doi.org/10.1103/PhysRevB.52.9970.
29. Lu. Yuan, Yu. Haixuan, and R.D. Sisson: *Mater. Sci. Eng. A*, 2017, vol. 700, pp. 592–97. https://doi.org/10.1016/j.msea.2017.05.094.
30. H. Bhadeshia and R. Honeycombe: in *Steels Microstruct. Prop.*, 4th ed., Elsevier, 2017, pp. 135–77. https://doi.org/10.1016/B978-0-08-100270-4.00005-6.
31. D. Barbier: *Adv. Eng. Mater.*, 2014, vol. 16, pp. 122–27. https://doi.org/10.1002/adem.201300116.
32. L.F. Alvarez, C. Garcia, and V. Lopez: *ISIJ Int.*, 1994, vol. 34, pp. 516–21. https://doi.org/10.2355/isijinternational.34.516.
33. C. Garcia de Andres and L.F. Alvarez: *J. Mater. Sci.*, 1993, vol. 28, pp. 1264–68. https://doi.org/10.1007/BF01191962.
34. J.Y. Park and Y.S. Park: *Mater. Sci. Eng. A*, 2007, vol. 448–451, pp. 1131–34. https://doi.org/10.1016/j.msea.2006.03.134.
35. S.S. de Souza, P.S. Moreira, and G.L. de Faria: *Mater. Res.*, 2020, vol. 23, pp. 1–9. https://doi.org/10.1590/1980-5373-mr-2019-0570.
36. A. Ning, R. Gao, S. Yue, H. Guo, and L. Li: *Mater. Res. Express*, 2021, https://doi.org/10.1088/2053-1591/abd4b6.
37. D.V. Doane: *J. Heat. Treat.*, 1979, vol. 1, pp. 5–30. https://doi.org/10.1007/BF02833206.
38. R.A. Grange, C.R. Hribal, and L.F. Porter: *Met. Trans A*, 1977, vol. 8A, pp. 1775–85. https://doi.org/10.1007/BF02646882.
39. G. Krauss: *Mater. Sci. Eng. A*, 1999, vol. 273–275, pp. 40–57. https://doi.org/10.1016/S0921-5093(99)00288-9.
40. A. Wiengmoon, T. Chairuangsri, and J.T.H. Pearce: *ISIJ Int.*, 2004, vol. 44, pp. 396–403. https://doi.org/10.2355/isijinternational.44.396.